Bulletin of Engineering Geology and the Environment (2022) 81: 244
https://doi.org/10.1007/s10064-022-02719-7

ORIGINAL PAPER

Shear behavior of sliding zone soil of loess landslides via ring shear tests in the South Jingyang Plateau

Rongsen Zhu[1] · Wan-li Xie[1] · Qiqi Liu[1] · Hui Yang[1] · Qiyao Wang[2]

Received: 14 May 2021 / Accepted: 20 April 2022 / Published online: 23 May 2022

Abstract

Since the 1970s, a large number of loess collapses and landslides have occurred in the Loess Plateau of China due to water diversion and irrigation projects. A large amount of ancient landslide deposits are accumulated at the foot of the tableland, which is likely to slide again in the case of a rapid increase in short-term rainfall or long-term irrigation. The weak characteristics of the sliding zone soil often become the key factor affecting the revival of old landslides. To explore the effects of water content and shear rate on shear behavior of the sliding zone soil, a series of ring shear tests were conducted on reconstituted loess in the South Jingyang Plateau. Experimental results suggest that under the condition of normal consolidation, the soil sample with the optimum moisture content has the highest shear strength. The increase in the shear rate effectively reduces the strength of the soil. Because of the high shear rate, the pore water that cannot be dissipated and fine particles accumulated at the shear plane form a weak base (slurry making theory), which cannot be easily stopped once the landslides start, leading to high-speed and long-distance landslides. In addition, the changes in the soil particles and pores were observed using a scanning electron microscope (SEM), and the observations were consistent with macroscopic results. From these studies, we come to the conclusion that the motion mechanism of reactivated landslide was associated with the interaction of water content and shear rate, which reduces the shear strength of the displaced materials to a great extent.

Keywords Loess landslide · Sliding zone soil · Shear behavior · Ring shear test · Microstructure

Introduction

In recent decades, in the Loess Plateau of Shaanxi and other places in China, water conservancy and hydropower projects have received increasing attention to improve agricultural production, well-being of people's lives, and economic development in the loess area; thus, a large number of water diversion and irrigation projects have been completed or are under construction. Although water diversion and irrigation projects meet the needs of cultivated land, they also change the natural geologic environment of the irrigation area, destroy internal water and soil balance and external ecological balance of the irrigation area, and cause a large number of environmental and geological problems such as landslides, collapses, soil salinization, soil erosion, land desertification, and ground subsidence (Guo et al. 2019; Ma et al. 2019; Yan et al. 2019). These problems greatly reduce the benefits of water conservancy and irrigation projects and affect the sustainable development of agriculture in the irrigation area. They also bring threats and losses to the life and property of the residents. A series of geological disasters caused by agricultural irrigation and their recurrence have recently attracted the attention of the government and researchers (Duan et al. 2019; Leng et al. 2018; Peng et al. 2018; Yuan et al. 2019).

Reactivated landslide is a common type in large-scale ancient landslide group. The rise and fall of groundwater level caused by rainfall (Li et al. 2020; Wang et al. 2020), irrigation (Lian et al. 2020), and reservoir impoundment (Guo et al. 2020a, b, c; Luo et al. 2019), the gravitational deformation of weak basement shear zone (Segui et al. 2020), and human engineering activities such as high-speed railway construction (Dhakal et al. 2020; Pando et al. 2020) will cause the stress redistribution and even instability of ancient landslide

✉ Wan-li Xie
xiewanli@nwu.edu.cn

[1] State Key Laboratory of Continental Dynamics, Department of Geology, Northwest University, Xi'an 710069, Shaanxi, China

[2] School of Civil Engineering, Chang'an University, Xi'an, Shaanxi 710054, China

accumulation. At present, the research on reactivated landslide mainly uses remote sensing (RS) (Guo et al. 2020a, b, c), interferometric SAR (InSAR) (Hearn et al. 2020; Xie et al. 2020), unmanned aerial vehicle (UAV) (Piroton et al. 2020), and other means to monitor the ancient landslide accumulation and uses numerical simulation software to study the impact of different trigger factor combinations on landslide risk evolution and make evaluation (Ren et al. 2020). With the deepening of research, the development characteristics and reactivation mechanism of ancient landslides are gradually revealed (Garcia-Delgado 2020; Guo et al. 2020a, b, c; Zhang et al. 2020), and the prediction model for landslide displacement is also proposed (Du et al. 2020). However, due to the change of the original structure of the soil caused by the first sliding, the physical and mechanical properties of the accumulation body have changed to a certain extent compared with the undisturbed soil. Therefore, it is still necessary to further explore the characteristics of the displaced material of this kind of landslide, so as to reveal its role in the process of causing and promoting sliding.

As a type of soil shear equipment developed based on direct shear apparatus, ring shear apparatus is easy to operate and has high performance, especially in long displacement shear. With the popularity of the ring shear apparatus, studies in the fields of construction engineering and geological disaster prevention were conducted on various soils in different regions under different working conditions (Dang et al. 2019; Ha et al. 2020; Quang et al. 2018; Tan et al. 2020). In this study, the strength and deformation characteristics of the sliding zone soil of the loess landslides in the South Jingyang Plateau in Shaanxi Province were investigated under different water contents and shear rates. A series of ring shear tests were carried out under different normal stress levels. The change in the soil microstructure was analyzed to explain the behavior of loess on macro scale. The conclusions drawn from this study can be used as a reference in slope stability analysis for the selection of shear strength parameters of soil in the sliding zone of reactivated loess landslides induced by irrigation.

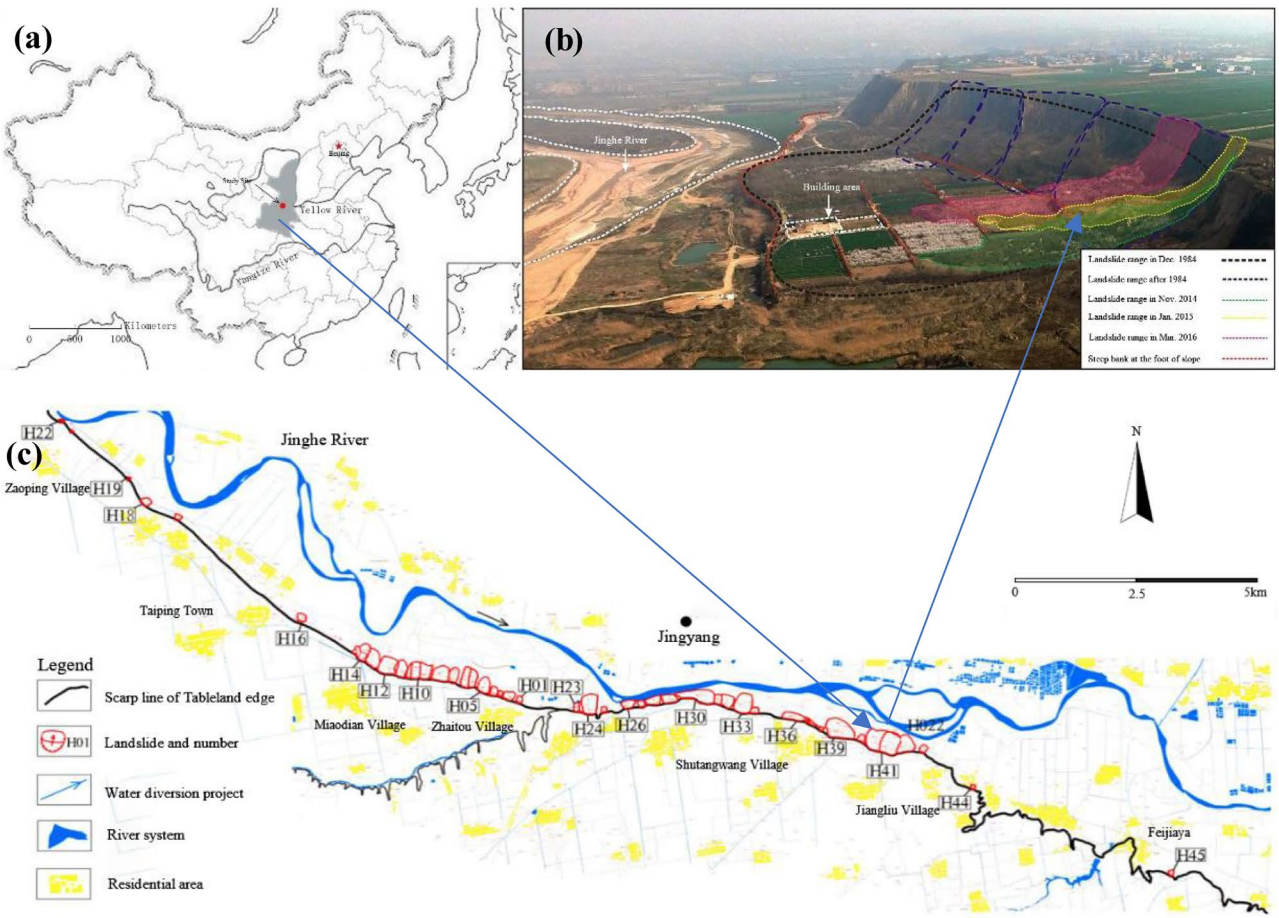

Fig. 1 (**a**) Location of the study site; (**b**) full view of the Jiangliu landslide; (**c**) distribution of the Jingyang landslide group

Study site

The Jiangliu landslide area is located in Jiangliu Village, Gaozhuang Town, Jingyang County (34°29′17.70″N, 108°51′44.32″E). Between the Dongfeng and Dabaozi landslide areas, the Jiangliu landslide area has the largest sliding range and causes the most severe disasters in the Jingyang landslide group (Fig. 1). In the last century, several landslides occurred in this area, in 1915, July 1982, December 1984, and December 1988. The sliding range in 1984 was the largest. The landslide moved 300 m toward the Jinghe River within 10 s, the main sliding direction was 7°, the sliding mass was 540 m wide from east to west, and the volume of the landslide was about 1.0×10^6 m^3. The landslide was a typical high-speed long-distance flow slide (Fig. 2). The landslide buried a village of 159 houses, destroyed more than 0.16 km^2 of arable land, and killed or injured 40 people. The landslide was reactivated in November 2014, January 2015, and March 2016, and the new deposits were imbricated on the old deposits.

According to the field investigation and exploration, the stratigraphic units where the landslide area is located comprise the following layers from the top to the bottom: (1) The Late Pleistocene aeolian loess Q_3^{eol} (Malan loess): It is 10.8-m-thick, yellowish brown, slightly wet, homogeneous soil, mainly composed of silt. It has needle-shaped pores, a small number of nodules, and some white stripes with collapsibility. (2) The Late Middle Pleistocene aeolian loess and paleosol sequence Q_2^{eol} (Lishi loess): It has a thickness of 70 m; the main stratum forms the slope; it is yellowish brown, homogeneous, mainly composed of silt; and it has needle-like pores, nodules, and snail shells, and vertical joints. Several layers of paleosols are brown–red and plastic and contain homogeneous soil nodules and a small amount of calcium. (3) The Early Middle Pleistocene alluvium Q_2^{al+pl}: It is distributed in the riverbed and floodplain of the Jinghe River. It is formed by alluvial and pluvial deposits of the Jinghe River and the thickness is 3–6 m. Most of the gravels are 5–10 cm in size, poorly sorted, and rounded. They form a distinct binary structure with the upper thin layer of loam and the lower layer of sandy soil.

The soil samples were taken from the slip plane of the Jiangliu landslide area. It was Lishi loess mixed with Malan loess and paleosols. In field measurements, the moisture content and density of the intact soil samples were detected as 16.7% and 1.75 g/cm^3, respectively. Table 1 shows the physical parameters of loess measured in laboratory tests.

Testing method

Ring shear test apparatus

Since Bishop et al. (1971) developed the first ring shear apparatus, different types of ring shear apparatus have appeared in succession. Sadrekarimi and Olson (2010) divided the ring shear apparatus into three types according to the position of the shear plane: the Sadrekarimi type with the shear plane at the bottom, the Bishop type with the shear plane in the middle, and the Bromhead type with the shear plane at the top. In recent years, new ring shear devices that can simulate more complex stress conditions have been developed (Jurko et al. 2008; Lourenco et al. 2006; Wang et al. 2007). Based on the development of these pieces of equipment, the mechanism of natural disasters such as

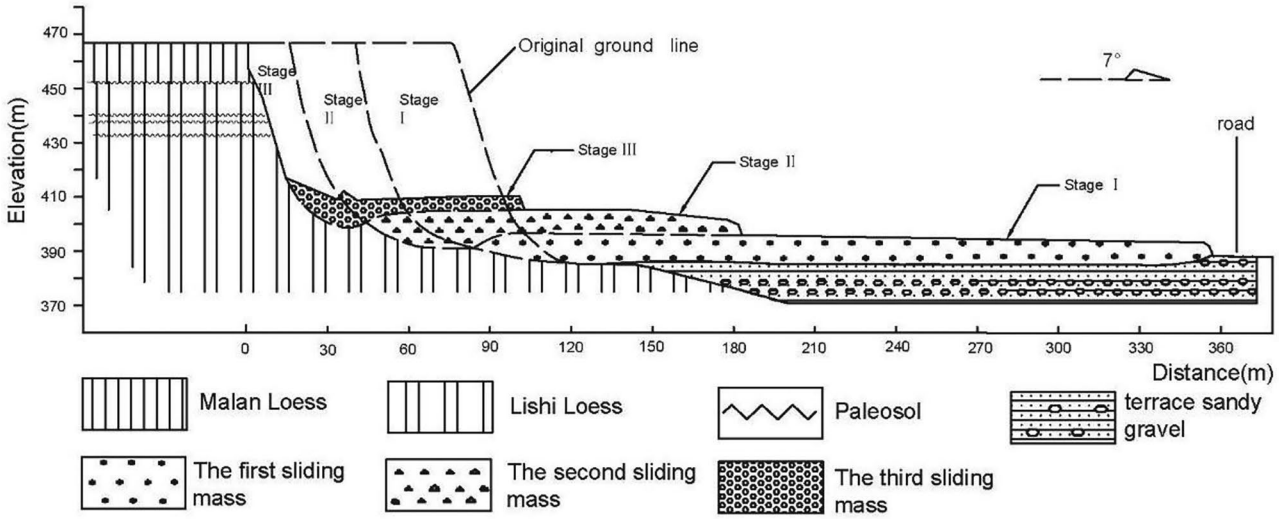

Fig. 2 Schematic geological cross-section of the Jiangliu landslide

Table 1 Physical parameters of loess at the sampling position

ω (%)	ρ (g/cm^3)	ρ_d (g/cm^3)	ω_L (%)	ω_P (%)	G_s (g/cm^3)	ω_{op} (%)	Grain content (%)		
16.7	1.75	1.50	28.73	13.68	2.7	14	< 0.005 mm	0.005–0.075 mm	> 0.075 mm
							16.13	80.02	3.85

ω natural water content, ρ density, ρ_d dry density, ω_L liquid limit, ω_p plastic limit, G_s specific gravity, ω_{op} optimum moisture content

landslides and debris flow is further revealed (Agung et al. 2004; Dang et al. 2016; Igwe et al. 2014).

The test equipment used in this study is SRS-150 ring shear apparatus produced by Geotechnical Consulting & Testing Systems (USA) (Fig. 3). It belongs to the Bromhead-type ring shear apparatus, and the shear plane appears in the upper part of the sample. During the test, vertical loading is maintained and the shear box is fixed. The soil sample is subjected to circumferential shear through the rotation of the vertical axis with the shear disk to obtain

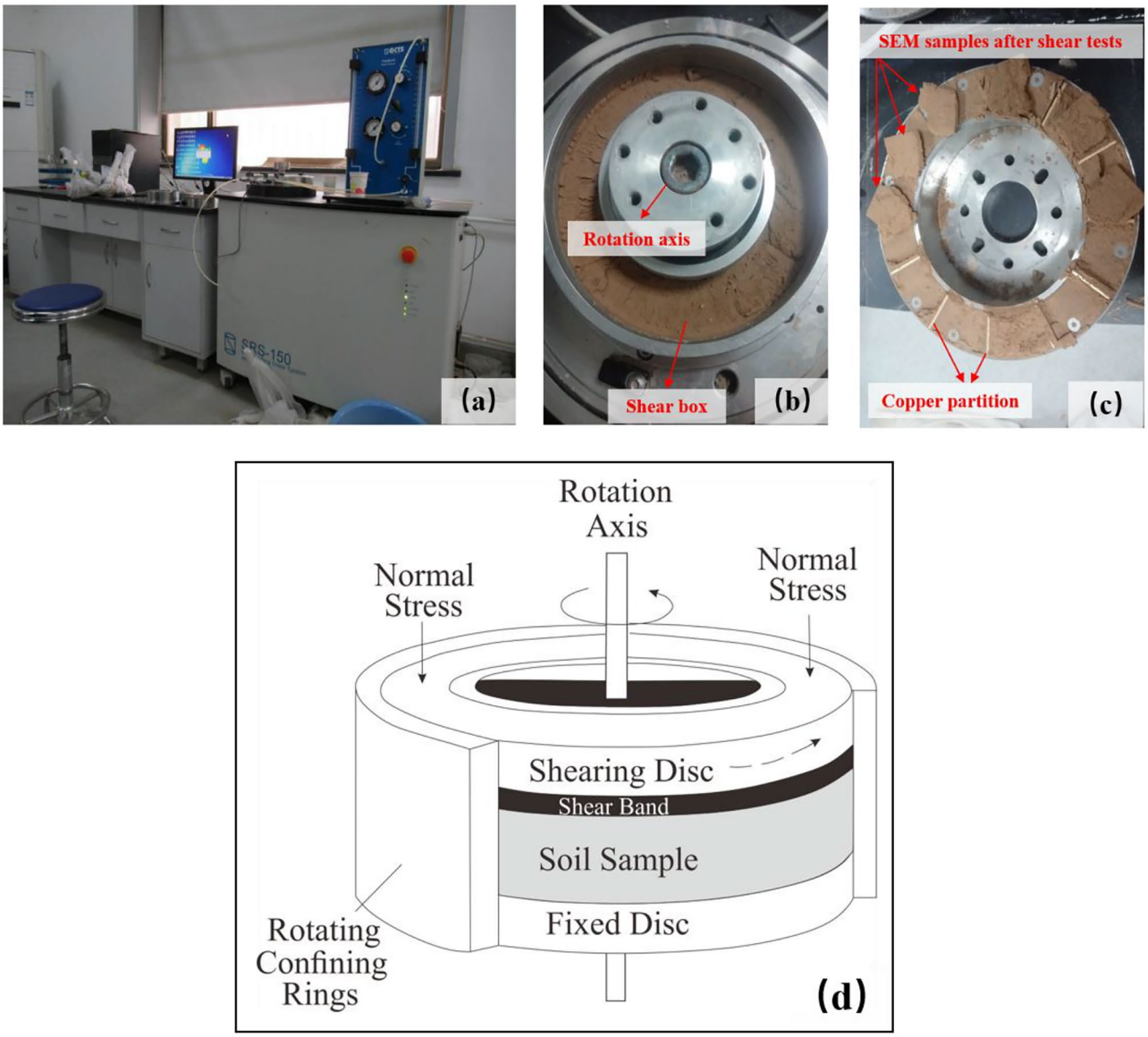

Fig. 3 (**a**) SRS-150 ring shear apparatus; (**b**) shear box; (**c**) shear disk (with SEM samples after ring shear tests); (**d**) schematic diagram of shearing

the shear strength and deformation of the soil. Copper diaphragms are embedded on the surface of the upper and lower walls contacting the soil samples to realize the predetermined shear plane and the internal shear of the soil. The inner diameter of the shear box is 96.5 mm, the outer diameter is 152.4 mm, the height of the sample is 25 mm, the maximum normal stress is 1000 kPa, and the peak shear stress is 1300 kPa. The shear speed is 0.001–360°/min. Fully automatic servo control and Harmonic Drive™ non-recoil driving technology are adopted to overcome the inherent recoil force phenomenon of the gear transmission device, and realize continuous rotation shear without intervals. In this way, continuous strain in the process of soil failure can be truly simulated, and the accuracy of the experiment is ensured. Compared with the DPRI or ICL ring shear instruments (Boldini et al. 2009; Sassa et al. 2014; Setiawan et al. 2016), SRS-150 cannot control the undrained shear surface at the upper of the soil sample, although it can achieve nondrainage at the bottom of the soil sample. Based on these factors, the tests in this study were conducted under consolidated drained shear conditions.

Testing procedure

It is difficult to make a circular intact sample of an appropriate size for a hollow torsional shear device. Skempton (1964) showed that the residual strength of soil is not related to the initial structure and stress history of soil, which provides a theoretical basis for using reconstituted samples to obtain the residual strength of soil. Therefore, reconstituted soil was used in the test, i.e., the loose soil was directly placed in the splicing box and formed by the consolidation of the shear disk. The soil samples collected from the field were passed through a 2-mm sieve (the maximum particle size was limited to 10% of the initial specimen height), placed in the oven, and completely dried at 105–110 °C. After cooling, water in different amounts was added according to the target moisture content and stirred until uniform. The larger aggregates were crushed, wrapped with preservative film, and placed in a moisturizing cylinder for 48 h, so as to fully transfer the water. To ensure the moisture content of the soil sample, debugging is required. In three different areas of the soil sample, 15–30 g of wet soil was placed in the aluminum boxes, and the current moisture content was calculated after soil is dry. If the difference between the current moisture content and the target moisture content is within the allowable range (±0.2%), the sample can be used directly; otherwise, there is soil water loss or other errors in soil preparation. In that case, the amount of soil or water that needs to be added again is determined, and the sample is wrapped with a preservative film and placed in the moisturizing cylinder for 48 h again.

After the prepared soil sample is placed into the shear box, the shear disk was installed, and the normal stress was applied to the soil sample by descending the disk. At the same time, the drainage valve was opened for drainage consolidation, and the consolidation time was controlled at 24 h at the set pressure. When high normal stress was applied to high water content soil sample, to prevent the soil sample from extrusion from the shear box, the loading rate of 0.08 kPa/s was set to 300 kPa in the program. After the consolidation procedure, soil samples were sheared using a single-stage shear test. At the end of the test, soil slices adhered to the shear disk were dried and removed for scanning electron microscopy (SEM) to analyze its microstructure.

Testing scheme

The natural moisture content of the soil sample was 16.7%. However, in field investigations, the maximum and minimum water contents of the sliding zone soil were 26.0% and 3.8%, respectively, which indicates that the water content of the soil changes greatly and controls the mechanical properties of the soil. In this study, the moisture content was 8%, 12%, 16%, 20%, and 24%. Considering the soil density and thickness, the normal stress values of 100, 200, and 300 kPa were selected, and the ring shear test with the rate of 10 mm/min was carried out under the drained condition. The shear rate of the ring shear test has great influence on soil strength; thus, it is the key factor to be considered. The influence of the shear rate on the shear strength of the sliding zone soil is complicated. Owing to the differences in soil properties and the limitations in test conditions, there has been no systematic explanation to date, but it is clear that the influence of shear rate can only be discussed within a relevant speed range to be meaningful (Wu et al. 2011). In laboratory tests, according to the influence of the shear rate on shear strength, < 1 mm/min is considered slow shear, 1–100 mm/min is medium-speed shear, and > 100 mm/min is fast shear (Li 2016). Based on the results of laboratory ring shear tests of natural soil samples, Lemos and Vaughan (2003) showed that the shear rate has three types of effects on residual strength: positive-rate effect (positive correlation between shear rate and residual strength), no-rate effect (no relationship between shear rate and residual strength), and negative-rate effect (negative correlation between shear rate and residual strength). Bhat and Yatabe (2015) showed that the residual strength changed little when the shear rate range was 0.073–0.233 mm/min and slightly increased when the rate was higher than 0.233 mm/min. By exploring the formation cause of the Yingong long-distance high-speed landslide, Hu et al. (2015) concluded that when the shear rate is less than 5.0 mm/s, the shear stress gradually decreases with the increase in the shear rate; when the shear rate is greater than 5.0 mm/s, the shear stress increases with the increase

in the shear rate. After considering the performance of the instrument and the actual conditions of the Jingyang landslide group, the samples at the saturated state were selected under the normal stress of 300 kPa to study the influence of shear rate on the failure process and the shear behavior of the sliding zone soil at the shear rates of 20, 40, 60, 80, and 100 mm/min.

Results and discussion

Strength property

In the whole test, most of the stress–strain curves show strain hardening without obvious peak and post-peak strain softening. The maximum strength usually occurs after the failure of the soil sample; thus, the peak value at the initial stage of the displacement is called initial strength. Figure 4 shows that under the same normal stress, the initial strength and residual strength increase first and then decrease with the increase in the water content, and the maximum value is obtained near the optimum moisture content. However, this is not only the contribution of the water content; for normal consolidated reconstituted soil, different water contents mean different compactness. If the water content is too low, there is only strong binding water in the soil, and the strong binding film is too thin; because of the friction between the particles, the soil particles cannot easily move and come close. If the water content is too high, there is free water in the soil. Under normal engineering load, the compressed part is the gas phase in the three phases of soil, and the solid particles and free water in the soil are considered to be incompressible. Free water in soil occupies a certain space; thus, the soil is not easily compacted. When the water content of the soil is optimal, there is a weakly bound water film in the soil, but there is no free water. The weakly bound

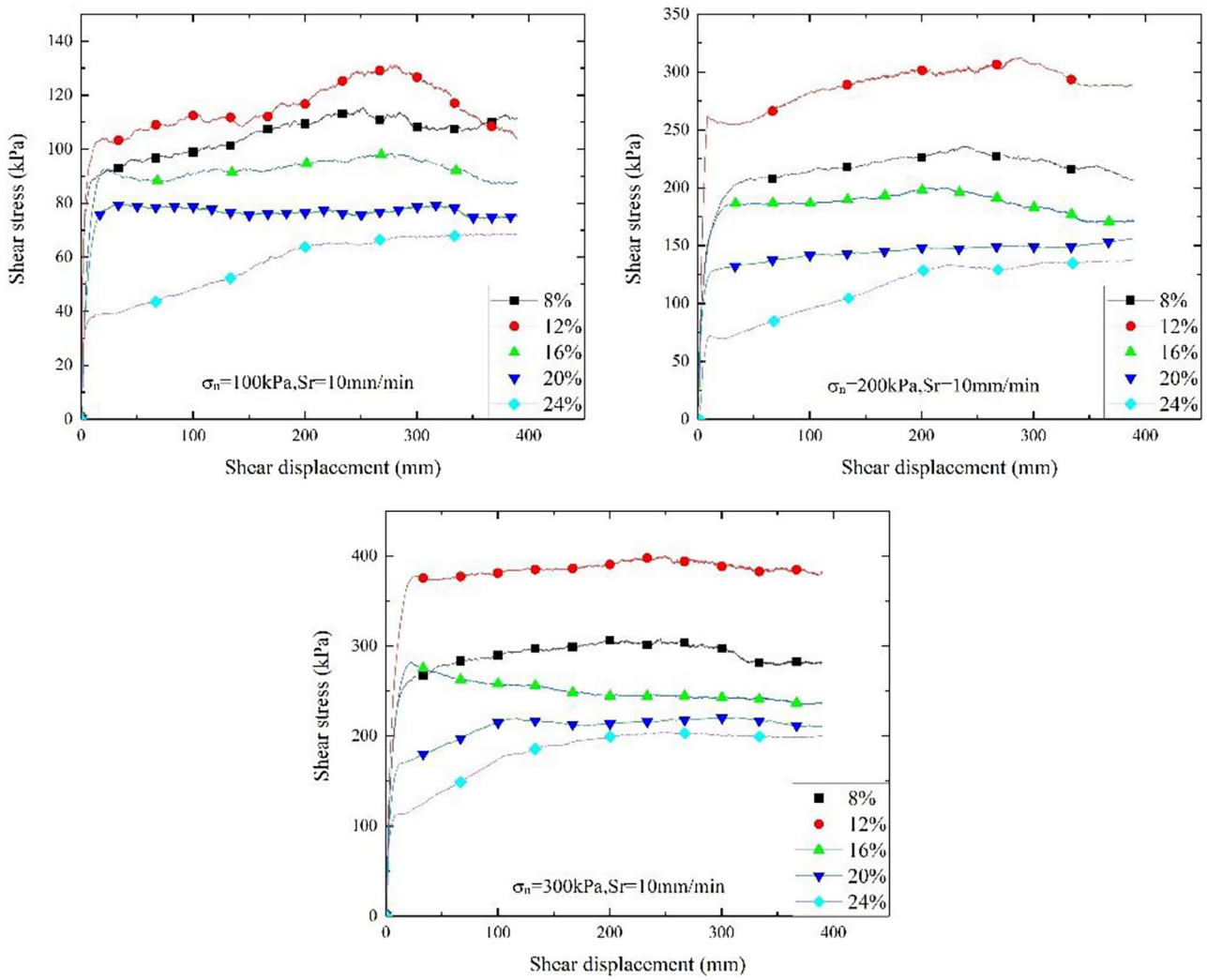

Fig. 4 Relationship between shear stress and shear displacement under different moisture contents

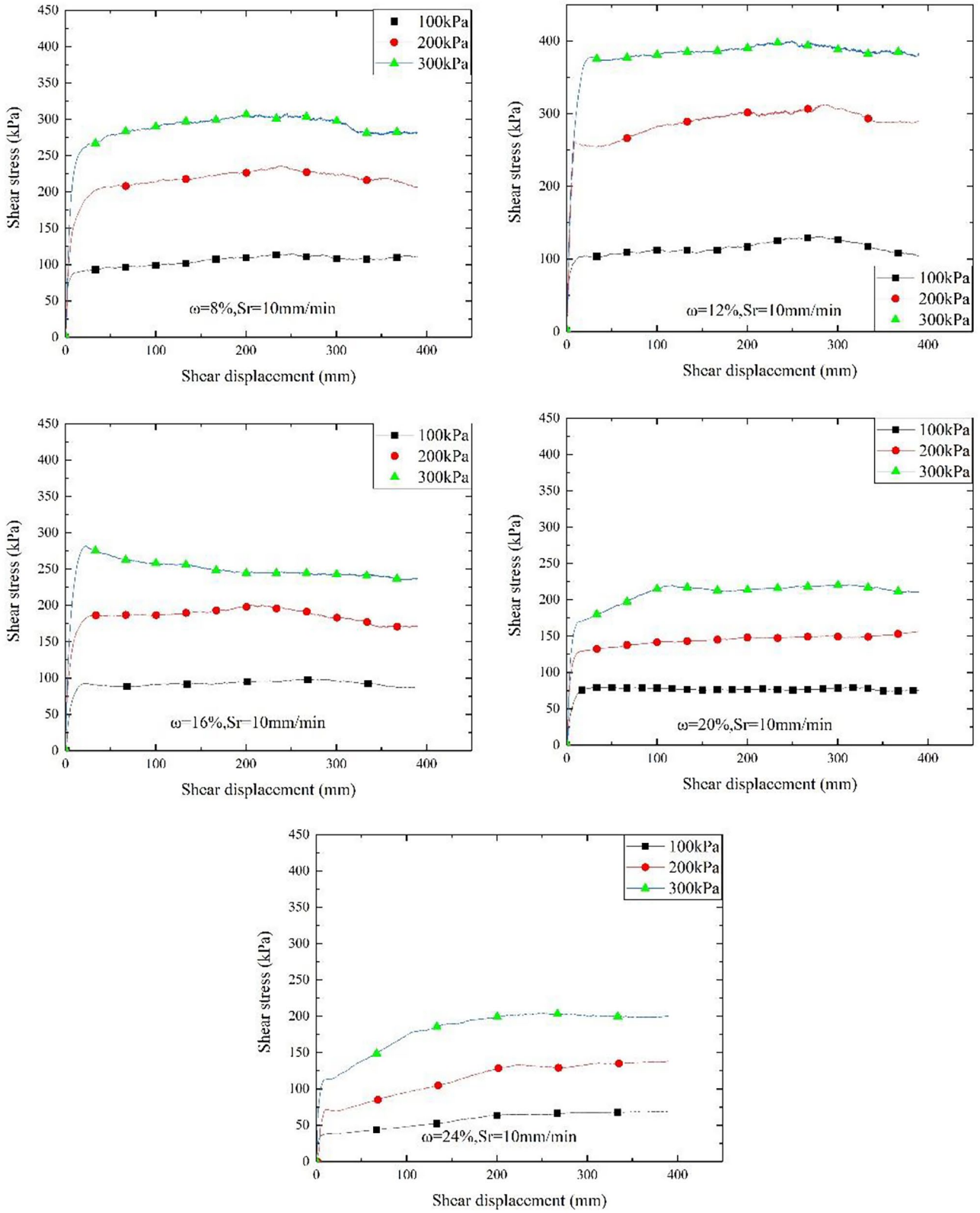

Fig. 5 Relationship between shear stress and shear displacement under different normal stresses

water film attached to the soil particles can move with the soil particles, which plays the role of lubrication, but does not prevent the soil particles from agglomerating; thus, soil can reach maximum compactness.

Under the same moisture content, the initial strength and residual strength are positively correlated with the normal stress. Compared with the low-stress state, the displacement required for the specimen with higher normal stress to reach the initial strength is shorter because the higher normal stress causes the soil sample to have higher compactness. Figure 5 shows that except for the sample with 16% water content showing strain softening under 300 kPa stress, the stress–strain curve of the soil shows the characteristics of strain hardening. The increase in strength caused by the increasing normal stress from 200 to 300 kPa is less than that from 100 to 200 kPa, which is evident under the low water content, which indicates the influence of normal stress is not a simple linear relationship. The Mohr–Coulomb criterion has its own scope of application.

To examine the influence of shear rate on residual strength, the test results of the saturated water content and normal stress of 300 kPa were taken as an example, the relationship between shear stress and shear displacement under different shear rates (Fig. 6) was determined, and the curves of shear stress and normal stress under unloading (Fig. 7) were drawn. Figure 6 shows that the shear stress decreases with the increase in the shear rate. The displacement required to reach the residual strength increases with the increase in the shear rate, which indicates that it takes a long time for the soil particles to complete the directional arrangement under high-speed shear likely because the shear plane under low speed transforms into the shear band under high speed (Fig. 8). The shear mode is not fixed; the increase in the shear rate may change the shear mode from the sliding type to the disturbed type because high speed increases the range and intensity of soil particle movement greatly, disturbs the original arrangement direction of flake particles, and reduces the orientation degree of the soil. Figure 7 and Table 2 show that the normal stress and shear stress maintain a strong linear relationship in the low-speed shear process, but there are fluctuations at the high speeds of 80 and 100 mm/min. The cohesion is not affected by the shear rate, but the internal friction angle is significantly reduced. The internal friction angle is 26.5° at 100 mm/min, which is 27.4% lower than 36.5° at 20 mm/min. The decrease in the internal friction angle indicates the failure of the large-particle soil on the shear plane and the filling of the pores by fine particles under high-speed shear.

Deformation property

Different from the dilatancy effect of coarse-grained soil under low normal stress, the samples in this test show shear shrinkage. Taking the samples with different shear rates as an example, we showed that with the progress of shear displacement, friction and compaction between soil particles intensified, resulting in vertical settlement. The larger the shear rate, the greater the settlement (Fig. 9). However, the decrease in the soil sample volume is not entirely caused by the decrease in pore volume. Due to the limitations of the instruments, the soil was extruded from the shear box during the shear process (Fig. 10). The higher the water content, the faster the shear rate, the more serious the soil extrusion. This is also a disadvantage of most ring shear instruments, especially for high-speed shear (> 100 mm/min). Therefore, the settlement of the soil sample with the shear rate of 100 mm/min is larger than the real value.

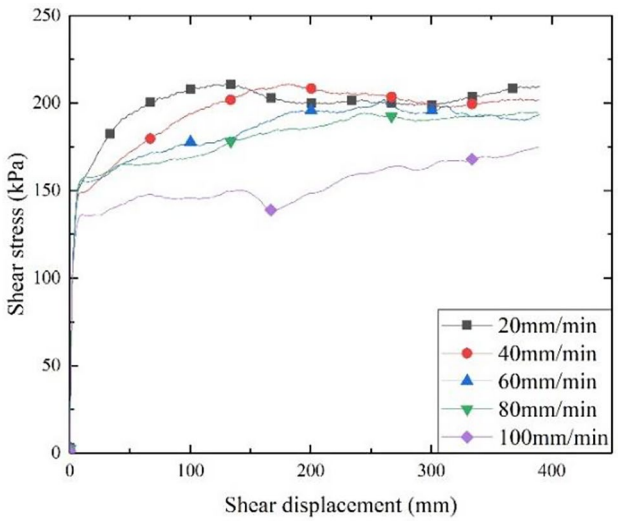

Fig. 6 Relationship between shear stress and shear displacement under different shear rates (saturated soil sample)

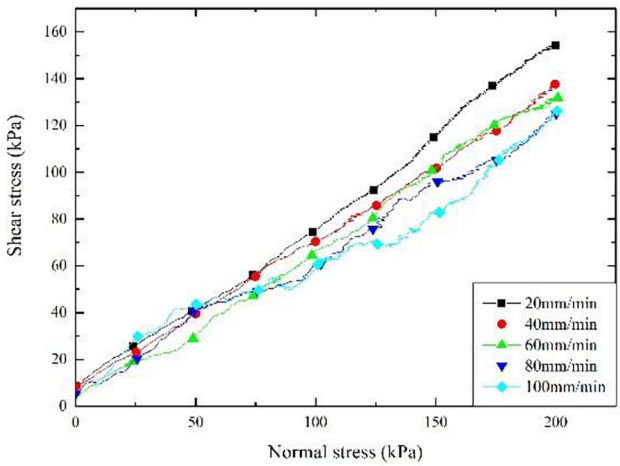

Fig. 7 Relationship between shear stress and normal stress under dynamic loading (saturated soil sample)

Fig. 8 (**a**) Smooth surface. (**b**) Non-smooth surface

When Skempton (1964) proposed the concept of residual shear strength, the drainage shear test was adopted. However, the study of the characteristics of the sliding zone soil indicated that there was no drainage condition in the process of landslides (Zhang and Wang 2018). Figure 11 shows the stress-shear displacement curve of the saturated sample at the shear rate of 100 mm/min. In the drained shear test, although the pore water pressure produced by slow shear can be dissipated in time during the shear process, if the shear rate is very high, the pore water pressure still exists even if it is drained shear. The higher shear rate makes the pore water pressure not dissipate in time, which leads to the migration of pore water to the shear plane; water content on the shear plane is significantly higher than that of the soil at other positions (Fig. 12). Due to the pressure difference between the rapidly rotating shear plane and the relatively stable soil below, the Bernoulli effect exerts suction on the shear plane, and smaller particles also migrate to the shear plane (stratification effect). Under the condition of drainage, the accumulation of water at the shear plane does not form liquefaction, and the shear strength of soil is greatly weakened but not completely lost. The fine particles formed by the broken particles at the shear plane and migrated due to the stratification effect are mixed with the pore water to form a weak foundation, supporting the sliding mass to slide for a longer distance.

Table 2 *C* and *Φ* of soil in sliding zone with different shear rates

Shear rates (mm/min)	C (kPa)	Φ (°)
20	8.6	36.5
40	8.1	32.4
60	4.2	33.9
80	5.4	26.8
100	8.6	26.5

Microstructure property

The change in the strength and deformation of soil is reflected not only at the macro level, but also in the microstructure. Since the microstructure of the loess was observed using the SEM, the stress–strain state of soil was studied from different aspects, and the changes in its physical and mechanical properties under natural disasters such as landslides, debris flow, and earthquakes

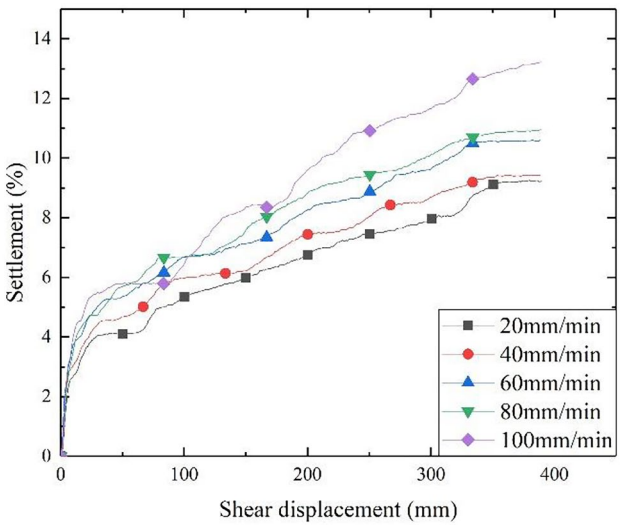

Fig. 9 Relationship between settlement and shear displacement under different shear rates

Fig. 10 Soil sample extruded from the shear box

Fig. 12 Accumulation of water at the shear plane

were explored (Li et al. 2019; Xie et al. 2018; Zhang et al. 2019). The SEM photos of ring shear specimens showed that soil particles have extrusion deformation and directional arrangement, and irregular step fractures (Fig. 13) are widely distributed on the shear plane, and their extension direction is roughly orthogonal to the shear displacement direction. In some samples, scratches (Fig. 14) consistent with the direction of shear displacement were observed. Through these fractures and scratches, we can explain further the micro-motion track of soil particles under macro-shear deformation. At higher shear rates, there are obvious bulges in the shear plane (Fig. 15). The disturbance caused by the high speed changes the shear plane (Fig. 8a) into a shear band with a certain thickness (Fig. 8b). A large number of skeleton particles near the shear plane can be observed by scanning electron microscopy at high magnification (Fig. 16), and most of the particles lose their clear boundaries. The open voids collapse, the fractures and embedded voids develop, and a large number of fine particles fill the pore. At the joint of the skeleton

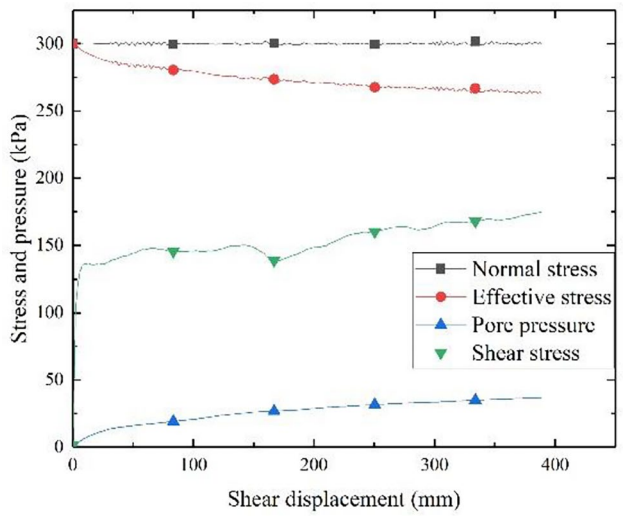

Fig. 11 Stress-shear displacement curve at the shear rate of 100 mm/min

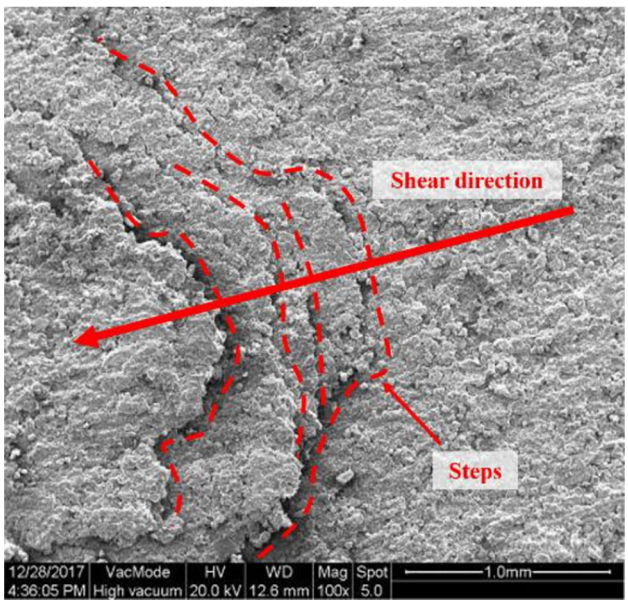

Fig. 13 Step fractures

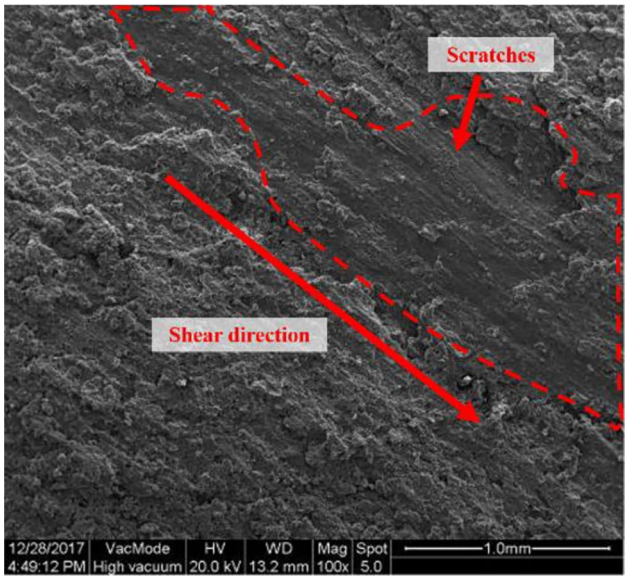

Fig. 14 Scratches

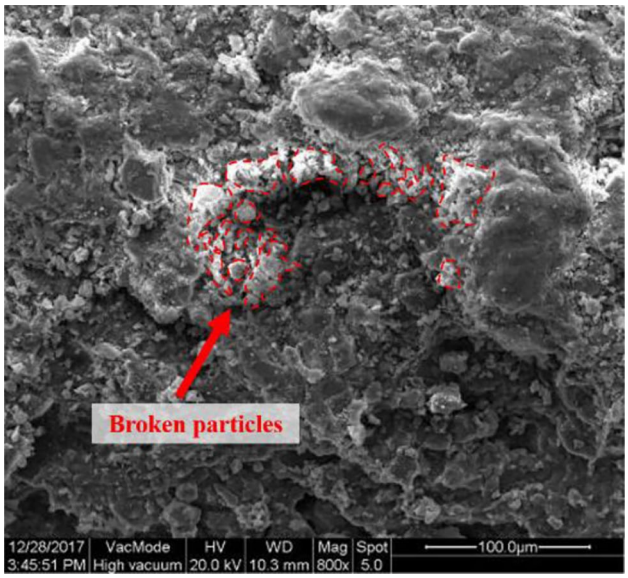

Fig. 16 Particle breakage of soil skeleton

particles, the bond strength of the cement controls the stability of the skeleton structure.

The SEM photos under different water contents (Figs. 17 and 18) show that higher water content can improve the roundness of skeleton particles and increase the contact area between particles, but the microstructure of loess has no obvious change, and the contact form and pore type of particles are still consistent with the state of low water content. Under a 100-fold view, samples with high water content show less directivity than those with low water content because the high water content makes soil aggregates bond with each other, reducing the number of gaps between aggregates to a certain extent, and thus making the number of steps less than that of samples with low water content. The Jingyang loess shows no or slight collapsibility under small stress but shows collapsibility under high stress. SEM photos under different normal stress values (Figs. 19 and 20) show that the microstructure of the loess changes little at low stress levels, which indicates that the internal structure of the

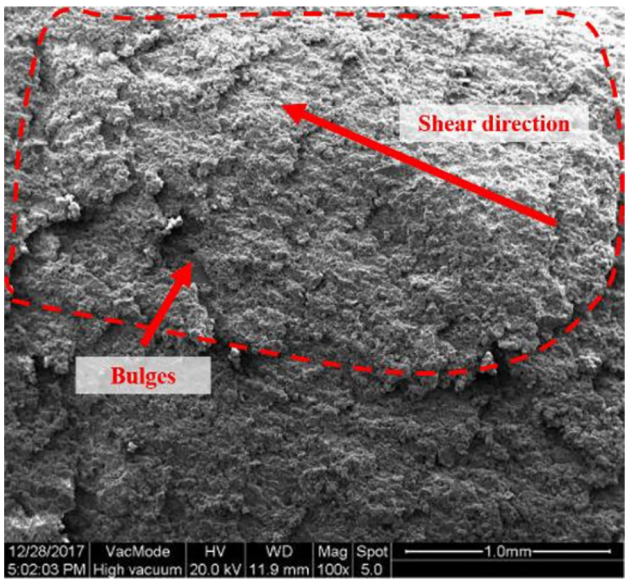

Fig. 15 Bulges

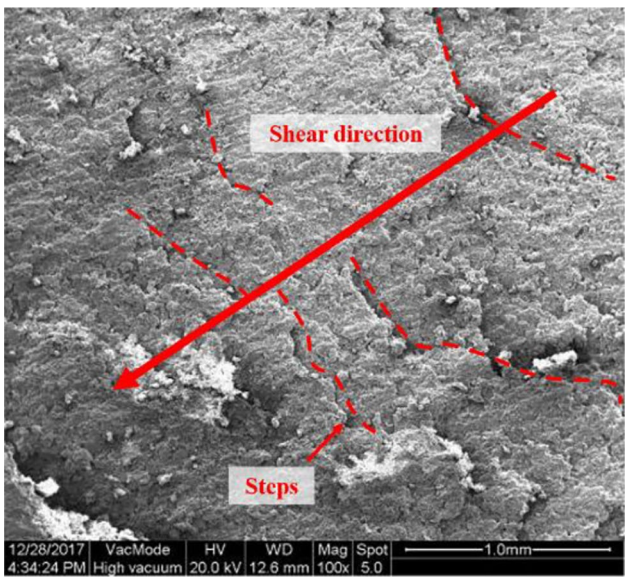

Fig. 17 Morphology of samples with low moisture content

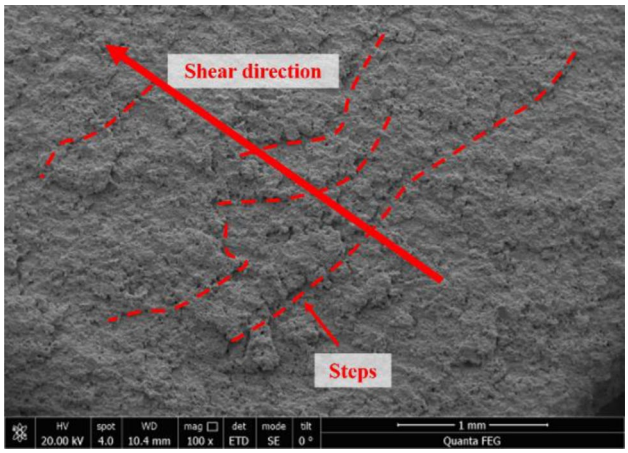

Fig. 18 Morphology of samples with high moisture content

loess can withstand the physical and mechanical changes caused by the external load at the low stress level, while at the high stress level, cementation cannot prevent the deformation of soil, a large number of skeleton particles are squeezed, the supporting structure is damaged, and the pores are invaded. Under the joint action of water and pressure, the skeleton particles move toward the pore direction and become part of the directional arrangement of soil.

Different from the reconstituted soil without shearing (Fig. 21), skeleton particles of the samples are mostly in contact with the dispersed flakes (Fig. 22), and the crevices and pores are developed. The broken clastic particles

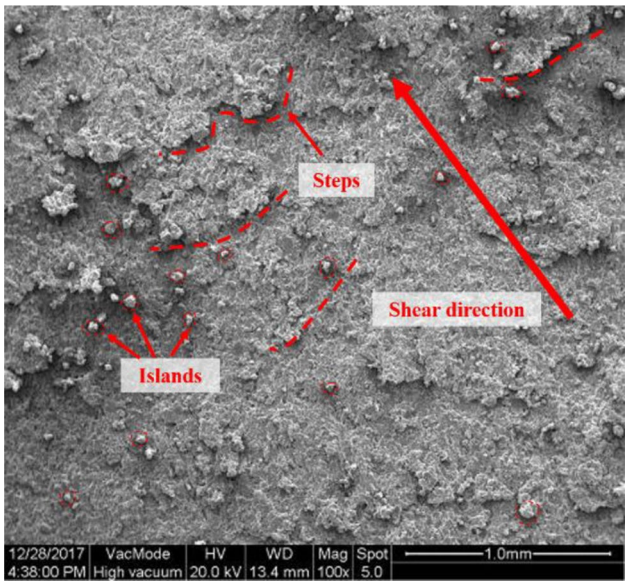

Fig. 19 Morphology of samples under low stress

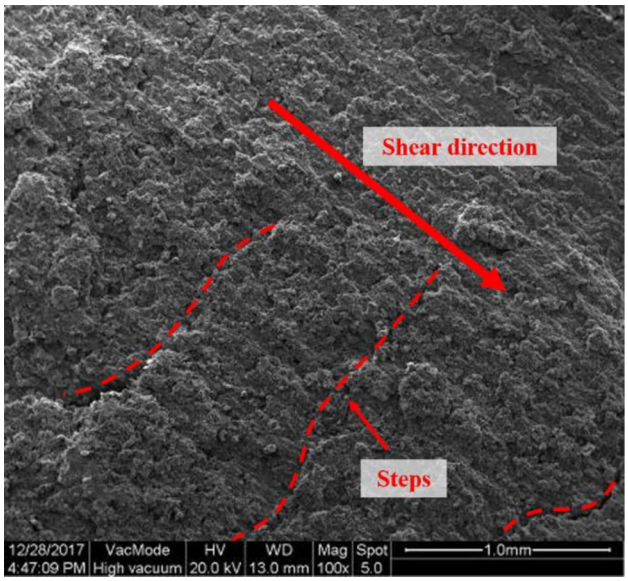

Fig. 20 Morphology of samples under high stress

and aggregate particles are staggered under the action of shear stress and occupy the original pore space. Because clastic particles have high strength and the aggregate also has certain strength, the relative displacement between skeletons needs to break through its own strength and connection strength, which requires a higher water content state or stress level. Pores in soil are not isolated, but coexist with soil skeleton. The skeleton supporting a certain pore is also the pillar of other adjacent pores. Once a certain pore collapses, it will cause a chain reaction of the collapse of adjacent pores. The skeleton and pores depend on each other. On the one hand, pores are generated between skeletons and are bound by skeletons, but they also limit

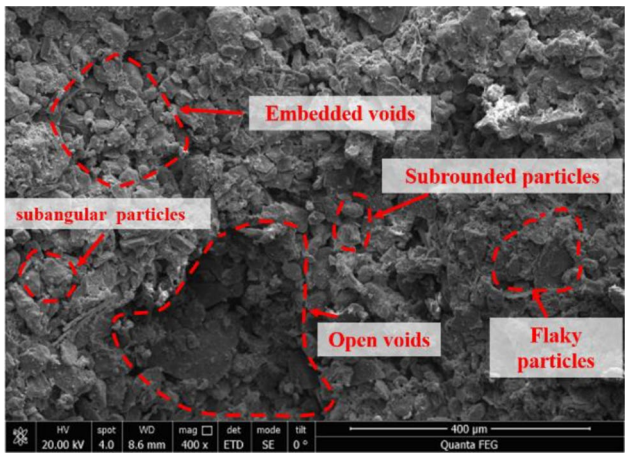

Fig. 21 Reconstituted soil skeleton structure without shearing

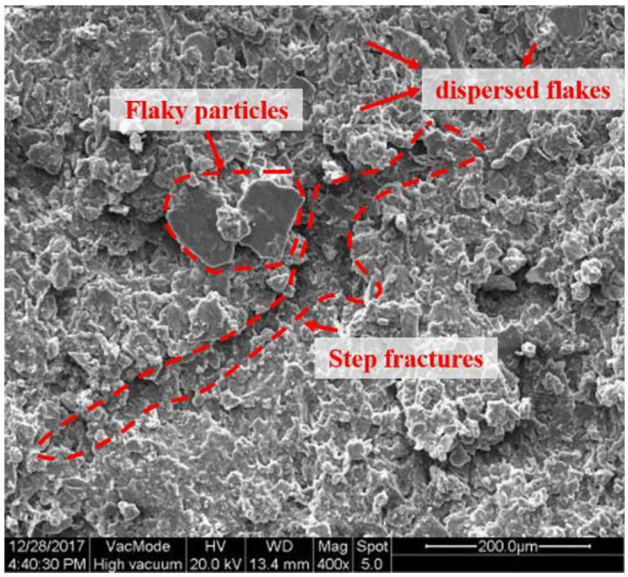

Fig. 22 Contact of dispersed flakes

the free movement space and the direction of the skeleton. On the other hand, the contact of skeleton particles breeds pores, but it has to invade the pore space to achieve stability under the influence of external factors. The continuous adjustment of the two makes the soil achieve temporary stability on macro scale.

Conclusions

The shear behavior of the loess sliding zone soil samples with different water content values under different normal stress and shear rate levels was studied via ring shear tests. The results can be summarized as follows.

1. It is a consensus that the strength of intact soil decreases monotonously with the increase of water content or the decrease of matrix suction; however, the situation in reconstituted soil has changed. Because different contents of water participate in the consolidation process, the reformed soil structure is greatly affected by the water content during consolidation. For the reconstituted soil with normal consolidation, the initial strength and residual strength first increase with the increase of water content, reach the maximum near the optimum moisture content, and then decrease. For the ancient landslides that have formed sliding surface, their strength is often controlled by the residual strength of the reconsolidated sliding zone soil. It is not recommended to use the strength of intact soil for the analysis of such landslides that may be reactivated. Although both of them and the primary landslides may fail at a higher moisture content, they have different mechanical properties in the whole process of moisture increase.
2. In the range of 20–100 mm/min, the shear strength decreases with the increase of shear rate, which indicates that once such landslide occurs, it is difficult to stop, i.e., such landslides are often catastrophic. Although the assumption of zero cohesion in residual state is generally accepted in engineering design, the residual cohesion is small but still exists even if the soil sample has been destroyed in drainage tests. This paper proves that the residual cohesion of reconstituted loess still exists through unloading test, which is consistent with the research of Tiwari et al. (2005). In the unloading test, the intercept of the stress–strain curve on the Y-axis is distributed in a very small range (4.2–8.6 kPa). Regardless of the inherent error of the instrument, it can be considered that the specimens with different shear rates have a similar residual cohesion value, that is, the shear rate has limited effect on the cohesion. On the other hand, the internal friction angle is greatly affected by the shear rate. From 20 to 100 mm/min, the internal friction angle decreases by 27.4%. The internal friction angle of soil reflects the friction characteristics of soil, including the sliding friction caused by the roughness of particle surface and the occlusal friction caused by the movement of particles due to the embedding, interlocking and disengagement of particles. The increase in shear rate makes these easier and reduces the value of internal friction angle. Based on the above, the effect of shear rate on the reduction of residual strength lies in the internal friction angle rather than the cohesion.
3. The SEM results show that the soil structure changes from isotropy to anisotropy. The shape of soil skeleton particles without shear is irregular, mostly angular, and the contact relationship is support contact or inlay contact. After shearing, most of the soil skeleton particles are in sheet shape and piled up in imbricate shape. The main contact form is face-to-face contact. The loss of friction caused by the occlusion between particles makes the shear stress lose the chance of further rising, and then become stable or decreasing. This contact form can well explain the macro sliding phenomenon and the critical state strength of soil. Under the shear condition, the soil particles are arranged along the shear direction. After a long enough shear displacement, the shape of soil particles and pore area gradually tend to be constant, which shows that the shear stress is constant, that is, the soil reaches the steady strength, that is, the residual strength.

Funding This study was financially supported by the National Natural Science Foundation of China (41972292, 41772323), the Innovation Capability Support Program of Shaanxi Province (2021TD-54),

the Key Research and Development Program of Shaanxi Province (2022ZDLSF06-03), the Shaanxi International Science and Technology Cooperation Program Key Project (2019KWZ-02), and the National Key R&D Program Project (2017YFD0800501).

References

Agung MW, Sassa K, Fukuoka H, Wang G (2004) Evolution of shear-zone structure in undrained ring-shear tests. Landslides 1(2):101–112

Bhat DR, Yatabe R (2015) Effect of shearing rate on residual strength of landslide soils. Engineering Geology for Society and Territory. Landslide Process 2:1211–1215

Bishop AW, Green GE, Garga VK, Andresen A, Brown JD (1971) A new ring shear apparatus and its application to the measurement of residual strength. Géotechnique 21(4):273–328

Boldini D, Wang F, Sassa K, Tommasi P (2009) Application of large-scale ring shear tests to the analysis of tsunamigenic landslides at the Stromboli volcano. Italy Landslides 6(3):231–240

Dang K, Sassa K, Fukuoka H, Sakai N, Sato Y, Takara K, Ha ND (2016) Mechanism of two rapid and long-runout landslides in the 16 April 2016 Kumamoto earthquake using a ring-shear apparatus and computer simulation (LS-RAPID). Landslides 13(6):1525–1534

Dang K, Sassa K, Konagai K, Karunawardena A, Bandara RM, Hirota K, Ha ND (2019) Recent rainfall-induced rapid and long-traveling landslide on 17 May 2016 in Aranayaka, Kagelle District. Sri Lanka Landslides 16(1):155–164

Dhakal S, Cui P, Rijal CP, Su LJ, Zou Q, Mavrouli O, Wu CH (2020) Landslide characteristics and its impact on tourism for two roadside towns along the Kathmandu Kyirong Highway. J Mt Sci-Engl 17(8):1840–1859

Du H, Song DQ, Chen Z, Shu HP, Guo ZZ (2020) Prediction model oriented for landslide displacement with step-like curve by applying ensemble empirical mode decomposition and the PSO-ELM method. J Clean Prod 270

Duan Z, Cheng W, Peng J, Wang Q, Chen W (2019) Investigation into the triggering mechanism of loess landslides in the south Jingyang platform. Shaanxi Province Bull Eng Geol Environ 78(7):4919–4930

Garcia-Delgado H (2020) The San Eduardo landslide (Eastern Cordillera of Colombia): reactivation of a deep-seated gravitational slope deformation. Landslides 17(8):1951–1964

Guo CB, Zhang YS, Li X, Ren SS, Yang ZH, Wu RA, Jin JJ (2020a) Reactivation of giant Jiangdingya ancient landslide in Zhouqu County, Gansu Province. China Landslides 17(1):179–190

Guo J, Xu M, Zhang Q, Xiao XX, Zhang SS, He SM (2020b) Reservoir regulation for control of an ancient landslide reactivated by water level fluctuations in Heishui River, China. J Earth Sci-China

Guo Q, Dai F, Zhao Z (2019) Analysis of the hydraulic properties of undisturbed layered loess in Northwest China. Water 11(7):1379

Guo ZZ, Chen LX, Yin KL, Shrestha DP, Zhang L (2020c) Quantitative risk assessment of slow-moving landslides from the viewpoint of decision-making: a case study of the Three Gorges Reservoir in China. Eng Geol 273

Ha ND, Sayama T, Sassa K, Takara K, Uzuoka R, Dang K, Van Pham T (2020) A coupled hydrological-geotechnical framework for forecasting shallow landslide hazard—a case study in Halong City. Vietnam Landslides 17(7):1–16

Hearn G, Larkin H, Papageorgiou A, Zoi GE (2020) Acceleration of the Pissouri landslide. Cyprus Q J Eng Geol Hydroge 53(4):530–541

Hu MJ, Pan HL, Zhu CQ, Wang FW (2015) High-speed ring shear tests to study the motion and acceleration processes of the Yingong landslide. J Mt Sci 12(6):1534–1541

Igwe O, Wang F, Sassa K, Fukuoka H (2014) The laboratory evidence of phase transformation from landslide to debris flow. Geosci J 18(1):31–44

Jurko J, Sassa K, Fukuoka H (2008) Study on seismic behavior of nonplastic silt by means of ring-shear apparatus. Landslides 5(2):189–201

Lemos LJ, Vaughan PR (2003) Shear behaviour of pre-existing shear zones under fast Loading-insights on the landslide motion. Proceedings of International Workshop: Occurrence and Earthfills, Sorrento and Mechanisms of Flow-like Landslides in Natural Slopes

Leng Y, Peng J, Wang Q, Meng Z, Huang W (2018) A fluidized landslide occurred in the Loess Plateau: a study on loess landslide in South Jingyang tableland. Eng Geol 236:129–136

Li P, Xie WL, Pak RY, Vanapalli SK (2019) Microstructural evolution of loess soils from the Loess Plateau of China. CATENA 173:276–288

Li WK (2016) Experiments of shear strength characteristics in ring shear tests of loess from South Jingyang Plateau. J Water Resour Archit Eng 14(1):184–187 (in Chinese)

Li WL, Zhao B, Xu Q, Yang F, Fu H, Dai C, Wu XX (2020) Deformation characteristics and failure mechanism of a reactivated landslide in Leidashi, Sichuan, China, on August 6, 2019: an emergency investigation report. Landslides 17(6):1405–1413

Lian BQ, Peng JB, Zhan HB, Huang QB, Wang XG, Hu S (2020) Formation mechanism analysis of irrigation-induced retrogressive loess landslides. Catena 195

Lourenco SD, Wang G, Sassa K, Fukuoka H (2006) Volumetric behavior of saturated sands under poor drainage conditions. J Geophys Res 111(F3)

Luo SL, Jin XG, Huang D (2019) Long-term coupled effects of hydrological factors on kinematic responses of a reactivated landslide in the Three Gorges Reservoir. Eng Geol 261

Ma P, Peng J, Wang Q, Duan Z, Meng Z, Jianqi Z (2019) Loess landslides on the South Jingyang Platform in Xi'an. China q J Eng Geol Hydrogeol 52(4):547–556

Pando L, Diaz-Diaz LM, Arias D, Castanon C, Lopez-Fernandez C (2020) A large palaeo-landslide reactivated by high-speed railway construction works (northern Spain). Q J Eng Geol Hydroge 53(2):290–297

Peng J, Ma P, Wang Q, Zhu X, Zhang F, Tong X, Huang W (2018) Interaction between landsliding materials and the underlying erodible bed in a loess flowslide. Eng Geol 234:38–49

Piroton V, Schlogel R, Barbier C, Havenith HB (2020) Monitoring the recent activity of landslides in the Mailuu-Suu Valley (Kyrgyzstan) Using Radar and Optical Remote Sensing Techniques. Geosciences 10(5)

Quang LH, Loi DH, Sassa K, Takara K, Ochiai H, Dang K, Ha DN (2018) Susceptibility assessment of the precursor stage of a landslide threatening Haivan Railway Station. Vietnam Landslides 15(2):309–325

Ren Y, Li TB, Dong SM, Tang JL, Xue DM (2020) Rainfall-induced reactivation mechanism of a landslide with multiple-soft layers. Landslides 17(5):1269–1281

Sadrekarimi A, Olson SM (2010) Shear band formation observed in ring shear tests on sandy soils. J Geotech Geoenviron Eng 136(2):366–375

Sassa K, Dang K, He B, Takara K, Inoue K, Nagai O (2014) A new high-stress undrained ring-shear apparatus and its application to the 1792 Unzen-Mayuyama megaslide in Japan. Landslides 11(5):827–842

Segui C, Rattez H, Veveakis M (2020) On the stability of deep-seated landslides. The Cases of Vaiont (Italy) and Shuping (Three Gorges Dam, China). J Geophys Res-Earth 125(7)

Setiawan H, Sassa K, Takara K, Miyagi T, Fukuoka H (2016) Initial pore pressure ratio in the earthquake triggered large-scale landslide near Aratozawa Dam in Miyagi Prefecture. Japan Procedia Earth Planet Sci 16:61–70

Skempton AW (1964) Long-Term Stability of Clay Slopes Géotechnique 14(2):77–102

Tan Q, Sassa K, Dang K, Konagai K, Karunawardena A, Bandara RMS, Tang H, Sato G (2020) Estimation of the past and future landslide hazards in the neighboring slopes of the 2016 Aranayake landslide. Sri Lanka Landslides 17(7):1727–1738

Tiwari B, Brandon TL, Marui H, Tuladhar GR (2005) Comparison of residual shear strengths from back analysis and ring shear tests on undisturbed and remolded specimens. J Geotech Geoenviron 131(9):1071–1079

Wang G, Sassa K, Fukuoka H, Tada T (2007) Experimental study on the shearing behavior of saturated silty soils based on ring-shear tests. J Geotech Geoenviron Eng 133(3):319–333

Wang HJ, Sun P, Zhang S, Han S, Li XB, Wang T, Guo Q, Xin P (2020) Rainfall-induced landslide in loess area, Northwest China: a case study of the Changhe landslide on September 14, 2019. Gansu Province Landslides 17(9):2145–2160

Wu D, Jian WB, Xu C (2011) Research on shear strength of residual soils by ring shear tests. Rock Soil Mech 32(7):2045–2050

Xie ML, Zhao WH, Ju NP, He CY, Huang HD, Cui QH (2020) Landslide evolution assessment based on InSAR and real-time monitoring of a large reactivated landslide, Wenchuan, China. Eng Geol 277

Xie WL, Li P, Vanapalli SK, Wang J (2018) Prediction of the wetting-induced collapse behaviour using the soil-water characteristic curve. J Asian Earth Sci 151:259–268

Yan R, Peng J, Huang Q, Chen L, Kang C, Shen Y (2019) Triggering influence of seasonal agricultural irrigation on shallow loess landslides on the South Jingyang Plateau. China Water 11(7):1474

Yuan W, Fan W, Jiang C, Peng X (2019) Experimental study on the shear behavior of loess and paleosol based on ring shear tests. Eng Geol 250:11–20

Zhang CY, Yin YP, Dai ZW, Huang BL, Zhang ZH, Jiang XN, Tan WJ, Wang LQ (2020) Reactivation mechanism of a large-scale ancient landslide. Landslides

Zhang F, Wang G (2018) Effect of irrigation-induced densification on the post-failure behavior of loess flowslides occurring on the Heifangtai area, Gansu. China Eng Geol 236:111–118

Zhang X, Lu Y, Li X, Lu Y, Pan W (2019) Microscopic structure changes of Malan loess after humidification in South Jingyang Plateau. China Environ Earth Sci 78(10):1–12